ChemComm

COMMUNICATION

View Article Online
View Journal | View Issue

Cite this: *Chem. Commun.*, 2019, 55, 13082

Received 23rd August 2019,
Accepted 5th October 2019

DOI: 10.1039/c9cc06556c

rsc.li/chemcomm

Ultrasensitive photoelectrochemical microRNA biosensor based on doxorubicin sensitized graphitic carbon nitride assisted by a target-activated enzyme-free DNA walker†

Yanlin Wang, Lingying Xia, Chongyao Wei, Haihua Wang, Haijun Wang, Ruo Yuan * and Shaping Wei*

Herein, a photoelectrochemical biosensor was successfully constructed on the basis of a sensitization strategy of doxorubicin sensitized graphitic carbon nitride for the ultrasensitive detection of microRNA-141 with the assistance of a target-activated enzyme-free DNA walker.

Photoelectrochemical (PEC) assays, as a promising analytical technique, have been developed rapidly owing to their unique advantages of low background signal, low cost and high sensitivity.[1–4] Until now, numerous works have focused on the excellent sensitization strategy based on the photoactive materials and appropriate sensitizers to broaden the light absorption range and promote the electron–hole separation, so as to obtain satisfactory analysis performance of biosensors.[5–9] Recently, various sensitization architectures have been extensively investigated, such as TiO_2/CdS:Mn/CdSeTe,[10] Au NPs/Bi_4NbO_8Cl,[11] BiOCl/Au/CdS QDs,[12] *etc.* Although the sensitizers above could effectively enhance the photoelectric conversion efficiency (PCE) of the basic photoactive materials, some deficiencies still exist, such as the high cost and limited loading amount of sensitizer. Hence, the exploration of a new sensitizer with low cost and preferable loading amount is highly desired. Doxorubicin (Dox), as a member of the anthracycline family, has been widely employed in cancer treatment[13,14] and biological detection.[15] For example, Ding and co-workers presented a novel drug carrier system based on loading Dox into DNA origami *via* intercalation for cancer treatment.[16] Fundamentally, Dox can be stably intercalated into the grooves of double-stranded DNA (dsDNA), resulting in a large amount of Dox in dsDNA.[17–19] More importantly, Dox with a calculated energy band gap (E_g) of about 2.14 eV (the calculation process is shown in the ESI†) could match well with graphitic carbon nitride (g-C_3N_4) with E_g of 2.7 eV.[20] Hence, it is expected to be exquisite using Dox as a photoactive sensitizer to fabricate a high PCE sensitization platform in the PEC field.

Recently, a number of autonomous DNA walkers, driven by the cleavage of various enzymes, have been extensively applied in the biological analysis field.[21–23] Although achieving high sensitivity, the enzymes used in these processes are readily degraded under adverse environmental conditions.[24] Consequently, researchers have focused on constructing enzyme-free DNA walkers in recent years. In these strategies, the autonomous movement of DNA walkers is mostly propelled by catalytic hairpin assembly (CHA)[25–27] and strand displacement reaction (SDR).[24,28] Compared with the enzyme-cleavage DNA walkers, enzyme-free DNA walkers have been regarded as a more valuable method due to the low cost, reliable control and easy construction. Inspired by these, a simple and effective target-activated enzyme-free DNA walker was reasonably designed in this work. In this proposed DNA walker, CHA replaced an enzyme to power the movement of the DNA walker exhibiting the features of being low cost and simple. Besides, the detection of other targets could be achieved by changing the recognition elements of the target. Ultimately, through the combination of a target-activated enzyme-free DNA walker and hybridization chain reaction (HCR), a considerable platform was successfully constructed for the loading of Dox to enhance the PCE of g-C_3N_4.

Herein, a PEC biosensor with the sensitization strategy of g-C_3N_4/Dox was proposed for the ultrasensitive detection of microRNA-141 (miRNA-141) with the assistance of a target-activated enzyme-free DNA walker. As shown in Scheme 1, g-C_3N_4 was employed as the basic photoactive material on the electrode surface. Next, hairpin DNA H1 and H2 were immobilized on the electrode surface. In the presence of target miRNA-141, H1 could hybridize with miRNA-141 to release the exposed tail sequence of H1 as a swing arm of the DNA walker for the opening

Key Laboratory of Luminescence and Real-Time Analytical Chemistry (Southwest University), Ministry of Education, College of Chemistry and Chemical Engineering, Southwest University, Chongqing 400715, P. R. China.
E-mail: yuanruo@swu.edu.cn, shapingw@swu.edu.cn; Fax: +86-23-68253172; Tel: +86-23-68252277

† Electronic supplementary information (ESI) available: Materials and reagents, apparatus, polyacrylamide gel electrophoresis (PAGE), experimental section, PEC measurement procedure, electrochemical characterizations of the PEC biosensor, optimal conditions of the PEC assay, the energy band gap (E_g) computational process for Dox, PAGE analysis, the reproducibility of the biosensor, and the feasibility of the developed biosensor in real samples. See DOI: 10.1039/c9cc06556c

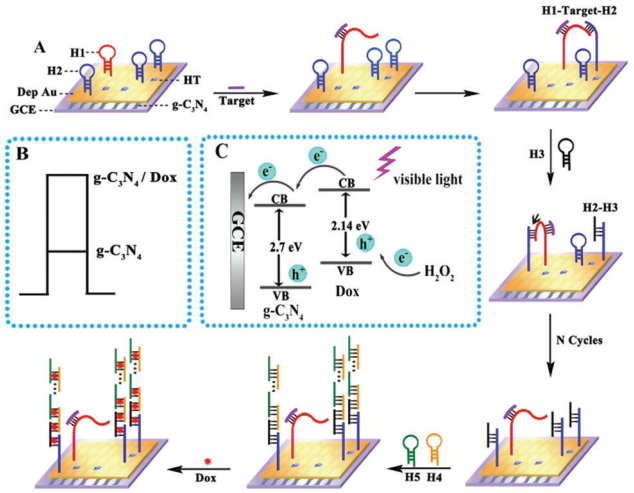

Scheme 1 Schematic illustration of (A) the biosensor construction process; (B) the signal comparison; (C) the photocurrent generation mechanism.

of hairpin DNA H2, thereby forming a H1-target-H2 complex. Then, the swing arm could be released again and hybridized with the other H2 to perform a cyclic reaction through a CHA process. After N cycles, a large number of H2–H3 complexes were formed on the electrode and then the exposed tail of H3 could open H4 for exposing the tail of H4. The exposed tail of H4 could further react with H5 to form a HCR circuit, leading to the generation of long dsDNA copolymers, which were used to provide numerous cavities for the loading of Dox. Ultimately, Dox was intercalated into the grooves of dsDNA, resulting in an enhanced photocurrent signal. This proposed PEC biosensor developed a simple and effective method for the ultrasensitive detection of biomarkers and provided a great potential application for early disease diagnosis.

The morphology characterization of the obtained g-C_3N_4 was recorded by scanning electron microscopy (SEM). The low-magnification SEM image in Fig. 1A exhibited a wrinkled surface and a typical stacked laminar structure of g-C_3N_4, but there were some small particles on the surface, which was attributed to partial agglomeration. The high-magnification SEM image in Fig. 1B showed a loose and porous structure of g-C_3N_4, which was similar to the tremella. From the ultraviolet-visible (UV-vis) absorption spectrum, the characteristic absorption peak of g-C_3N_4 was at approximately 322 nm (Fig. 1C), which was nearly consistent with the reported value in the previous literature.[29] Meanwhile, according to Fig. 1D, Dox displayed an obvious adsorption peak at about 480 nm, corresponding to the earlier report.[30]

The photocurrent signal was applied to analyze the construction process of the PEC biosensor. As displayed in Fig. 2, the photocurrent signal of the bare glassy carbon electrode (GCE) nearly closed to zero (curve a). When g-C_3N_4 was dropped on the electrode, the photocurrent signal was increased obviously (curve b). Sequentially, the photocurrent signal was further increased (curve c) after the electrodeposition of the gold nanoparticle layer (Dep Au) due to the excellent conductivity of Dep Au. After the obtained electrode was stepwise modified with the mixture solution of H1 and H2, hexanethiol (HT), target, H3, and a mixture solution of H4 and H5, the photocurrent signal decreased successively (curve d, e, f, g, and h, respectively) on account of the increased steric hindrance effect of DNA and HT. Finally, the photocurrent signal obviously increased (curve i) with the addition of Dox, because Dox could be intercalated into the grooves of dsDNA and increase the PCE of g-C_3N_4. The above results proved that the PEC biosensor was constructed successfully.

The analytical performance of the proposed PEC biosensor was estimated by detecting various concentrations of the target under optimized conditions (Fig. S2, ESI†). The photocurrent responses for the target with various concentrations are recorded in Fig. 3. According to Fig. 3A, the PEC signals constantly increased along with incremental target concentrations over the range of 0.25 fM–2.5 nM. Based on the photocurrent signals and the logarithm of miRNA-141 concentration (Fig. 3B), the line regression equation was $I = 0.2352 \lg c_{target} + 1.186$ ($r = 0.9944$), and in this equation, I is the PEC signal, c is the concentration of miRNA-141 and r is the correlation coefficient. Furthermore, the detection limit was 83 aM (S/N = 3). In addition, a comparison

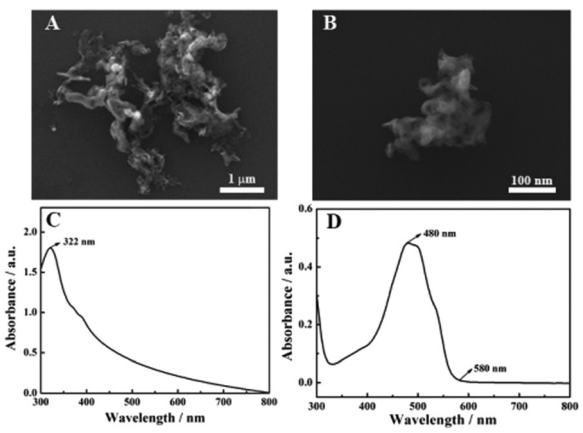

Fig. 1 SEM images of g-C_3N_4 under (A) low magnification and (B) high magnification. Typical UV-vis absorption spectrum of (C) g-C_3N_4 and (D) Dox.

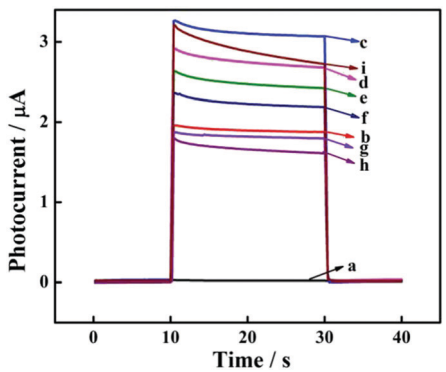

Fig. 2 PEC responses of each immobilized step: (a) bare GCE; (b) g-C_3N_4/GCE; (c) Dep Au/g-C_3N_4/GCE; (d) H1–H2/Dep Au/g-C_3N_4/GCE; (e) HT/H1–H2/Dep Au/g-C_3N_4/GCE; (f) target/HT/H1–H2/Dep Au/g-C_3N_4/GCE; (g) H3/target/HT/H1–H2/Dep Au/g-C_3N_4/GCE; (h) H4–H5/H3/target/HT/H1–H2/Dep Au/g-C_3N_4/GCE; (i) Dox/H4–H5/H3/target/HT/H1–H2/Dep Au/g-C_3N_4/GCE.

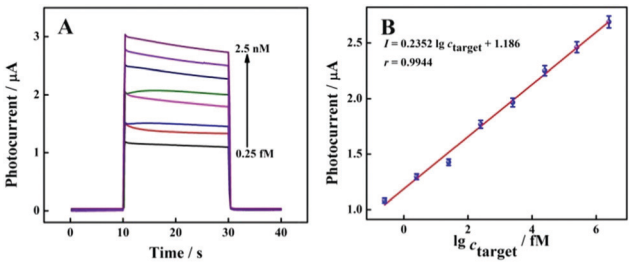

Fig. 3 (A) PEC responses of the biosensor incubated with miRNA-141 at different concentrations in 5 mL of PBS (0.1 M, pH 7.0) containing 50 μL of 30% hydrogen peroxide: 0.25 fM, 2.5 fM, 25 fM, 0.25 pM, 2.5 pM, 25 pM, 0.25 nM and 2.5 nM (from bottom to top). (B) The corresponding calibration curve for miRNA-141 detection.

study between the proposed PEC biosensor assay and the previously reported strategies is shown in Table S2 (ESI†). It was exhibited that the proposed PEC biosensor possessed a satisfactory analysis performance with a wider linear range and lower detection limit.

The selectivity of this biosensor was verified by using miRNA-122, miRNA-126 and miRNA-21 as interferences. As exhibited in Fig. 4A, compared to the photocurrent signal of miRNA-141 (2.5 pM), obviously weak signals were obtained from the interferences (0.25 nM), which indicated that the proposed PEC biosensor possessed a satisfactory selectivity. Besides, the stability of the PEC biosensor is illustrated in Fig. 4B. Under consecutive off–on–off light for 10 cycles, the relative standard deviation (RSD) was 0.99%, which revealed that the PEC biosensor possessed a commendable stability.

In summary, a PEC biosensor based on a sensitization structure of g-C_3N_4/Dox was established for the ultrasensitive detection of miRNA-141 based on a target-activated enzyme-free DNA walker. Since Dox could be stably embedded in the grooves of dsDNA, the loading amount of the sensitizer could be significantly increased. The effective combination between the photoactive material of g-C_3N_4 and the sensitizer of Dox was conducive to promoting the electron–hole separation and increasing the PCE of g-C_3N_4, leading to a remarkably enhanced PEC signal. Moreover, the target-activated enzyme-free DNA walker driven by CHA could trigger HCR to produce numerous dsDNA grooves for significantly improving the loading amount of Dox. The proposed PEC biosensor exhibited a wide linear range, superior stability and good selectivity for miRNA detection, which provided a potential application in bioanalysis and disease diagnosis.

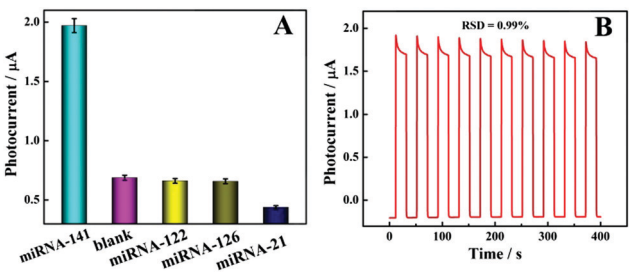

Fig. 4 (A) Selectivity of the proposed strategy toward different samples: miRNA-141 (2.5 pM), miRNA-122 (0.25 nM), miRNA-126 (0.25 nM), and miRNA-21 (0.25 nM). (B) Stability of the proposed strategy incubated with miRNA-141 (0.25 pM).

This work was financially supported by the National Natural Science Foundation (NNSF) of China (21575116, 21675129, 21775124 and 21974108) and the Fundamental Research Funds for the Central Universities (XDJK2018AA003), China.

Conflicts of interest

There are no conflicts to declare.

Notes and references

1 W. W. Zhao, J. J. Xu and H. Y. Chen, *Chem. Rev.*, 2014, **114**, 7421–7441.
2 Q. Hao, X. Shan, J. Lei, Y. Zang, Q. Yang and H. Ju, *Chem. Sci.*, 2016, **7**, 774–780.
3 T. Hou, N. N. Xu, W. X. Wang, L. Ge and F. Li, *Anal. Chem.*, 2018, **90**, 9591–9597.
4 L. Y. Xia, M. J. Li, H. J. Wang, R. Yuan and Y. Q. Chai, *Chem. Commun.*, 2019, **55**, 9721–9724.
5 C. Ye, M. Q. Wang, H. Q. Luo and N. B. Li, *Anal. Chem.*, 2017, **89**, 11697–11702.
6 Q. M. Shen, L. Han, G. C. Fan, J. R. Zhang, L. P. Jiang and J. J. Zhu, *Anal. Chem.*, 2015, **87**, 4949–4956.
7 Y. H. Zhang, Y. N. Zheng, M. J. Li, T. Hu, R. Yuan and S. P. Wei, *Anal. Chem.*, 2018, **90**, 12278–12283.
8 Y. X. Chu, A. P. Deng, W. J. Wang and J. J. Zhu, *Anal. Chem.*, 2019, **91**, 3619–3627.
9 R. Y. Yang, K. Zou, X. H. Zhang, C. C. Du and J. H. Chen, *Chem. Commun.*, 2019, **55**, 8939–8942.
10 G. C. Fan, H. Zhu, D. Du, J. R. Zhang, J. J. Zhu and Y. H. Li, *Anal. Chem.*, 2016, **88**, 3392–3399.
11 Y. F. Ruan, N. Zhang, Y. C. Zhu, W. W. Zhao, J. J. Xu and H. Y. Chen, *Anal. Chem.*, 2017, **89**, 7869–7875.
12 R. J. Zeng, Z. B. Luo, L. S. Su, L. J. Zhang, D. P. Tang, R. Niessner and D. Knopp, *Anal. Chem.*, 2019, **91**, 2447–2454.
13 F. Yang, T. T. Zhang, S. S. Li, P. Song, K. Zhang, Q. Y. Guan, B. Kang, J. J. Xu and H. Y. Chen, *Anal. Chem.*, 2017, **89**, 10239–10247.
14 F. J. Yao, J. Duan, Y. Wang, Y. Zhang, Y. L. Guo, H. L. Guo and X. F. Kang, *Anal. Chem.*, 2015, **87**, 338–342.
15 F. Patolsky, E. Katz and I. Willner, *Angew. Chem., Int. Ed.*, 2002, **41**, 3398–3402.
16 Q. Jiang, C. Song, J. Nangreave, X. W. Liu, L. Lin, D. L. Qiu, Z. G. Wang, G. Z. Zou, X. J. Liang, H. Yan and B. Q. Ding, *J. Am. Chem. Soc.*, 2012, **134**, 13396–13403.
17 V. Bagalkot, O. Farokhzad, R. Langer and S. Y. Jon, *Angew. Chem., Int. Ed.*, 2006, **45**, 8149–8152.
18 B. Jawad, L. Poudel, R. Podgornik, N. F. Steinmetze and W. Y. Ching, *Phys. Chem. Chem. Phys.*, 2019, **21**, 3877–3893.
19 K. Nawara, P. Krysinski and G. J. Blanchard, *J. Phys. Chem. A*, 2012, **116**, 4330–4337.
20 W. J. Ong, L. L. Tan, Y. H. Ng, S. T. Yong and S. P. Chai, *Chem. Rev.*, 2016, **116**, 7159–7329.
21 J. L. Liu, Z. L. Tang, J. Q. Zhang, Y. Q. Chai, Y. Zhuo and R. Yuan, *Anal. Chem.*, 2018, **90**, 5298–5305.
22 X. L. Yang, Y. N. Tang, S. D. Mason, J. B. Chen and F. Li, *ACS Nano*, 2016, **10**, 2324–2330.
23 Z. Q. Xu, L. L. Liao, Y. Q. Chai, H. J. Wang and R. Yuan, *Anal. Chem.*, 2017, **89**, 8282–8287.
24 W. Liu, A. Y. Chen, S. K. Li, K. F. Peng, Y. Q. Chai and R. Yuan, *Anal. Chem.*, 2019, **91**, 1516–1523.
25 C. Jung, P. B. Allen and A. D. Ellington, *Nat. Nanotechnol.*, 2016, **11**, 157–163.
26 W. Li, L. Wang and W. Jiang, *Chem. Commun.*, 2017, **53**, 5527–5530.
27 N. X. Li, J. Zheng, C. R. Li, X. X. Wang, H. X. Ji and Z. K. He, *Chem. Commun.*, 2017, **53**, 8486–8488.
28 L. C. Peng, P. Zhang, Y. Q. Chai and R. Yuan, *Anal. Chem.*, 2017, **89**, 5036–5042.
29 T. T. Pham and E. W. Shin, *Langmuir*, 2018, **34**, 13144–13154.
30 D. Y. Wu, H. S. Wang, X. S. Hou, H. Chen, Y. Ma, Y. L. Hou, J. Hong and Y. Ding, *Nano Res.*, 2018, **11**, 3396–3410.

